

Schlieren imaging of loud sounds and weak shock waves in air near the limit of visibility

Michael John Hargather · Gary S. Settles ·
Matthew J. Madalis

Received: 27 April 2009 / Accepted: 4 August 2009
© Springer-Verlag 2009

Abstract A large schlieren system with exceptional sensitivity and a high-speed digital camera are used to visualize loud sounds and a variety of common phenomena that produce weak shock waves in the atmosphere. Frame rates varied from 10,000 to 30,000 frames/s with microsecond frame exposures. Sound waves become visible to this instrumentation at frequencies above 10 kHz and sound pressure levels in the 110 dB (6.3 Pa) range and above. The density gradient produced by a weak shock wave is examined and found to depend upon the profile and thickness of the shock as well as the density difference across it. Schlieren visualizations of weak shock waves from common phenomena include loud trumpet notes, various impact phenomena that compress a bubble of air, bursting a toy balloon, popping a champagne cork, snapping a wooden stick, and snapping a wet towel. The balloon burst, snapping a ruler on a table, and snapping the towel and a leather belt all produced readily visible shock-wave phenomena. In contrast, clapping the hands, snapping the stick, and the champagne cork all produced wave trains that were near the weak limit of visibility. Overall, with sensitive optics and a modern high-speed camera, many nonlinear acoustic phenomena in the air can be observed and studied.

Communicated by B. W. Skews.

A more concise version of this manuscript was presented at the 13th International Symposium on Flow Visualization, Nice, France, 1–4 July 2008.

M. J. Hargather (✉) · G. S. Settles · M. J. Madalis
Penn State Gas Dynamics Laboratory, Pennsylvania State University,
301D Reber Building, University Park, PA 16802, USA
e-mail: mjh340@psu.edu

G. S. Settles
e-mail: gss2@psu.edu

M. J. Madalis
e-mail: mjmadalis@gmail.com

Keywords Shock waves · Nonlinear acoustics · Sound · Noise · Schlieren · High-speed imaging

PACS 42.79.Mt · 43.25.+y

1 Introduction

Visualizing sound-wave motion in air has been a dream of scientists and engineers for at least a century and a half, although sound waves and weak shock waves were initially confused. August Toepler's (1836–1912) epitaph, "He was the first to see sound," actually referred to his schlieren imaging of weak shock waves from electric sparks [1]. This error continued well into the twentieth century (e.g. [2,3]) before the distinction between linear sound and true shock waves finally became clear to all.

Whether described as sound or weak shock waves, many researchers through history have studied these weak waves and their motion. Wood explored weak shock wave reflection and refraction using electric sparks and schlieren visualization [4]. Sabine [5] later used shadowgrams of weak spark-driven shock waves in scale models to explore theater acoustics. More recently Kock [6] used an electromechanical scanning method to map sound patterns in air. The schlieren method became the standard means to image ultrasonic wave motion in water, e.g. [7], although that topic is beyond the present scope. Bucaro and Dardy [8] demonstrated in 1977 the schlieren imaging of ultrasonic waves in air at 200 kHz. Bershader and Prakash [9] calculated that a schlieren system with 1/5 arcsecond sensitivity could only image 1 kHz sound in air at a sound pressure level (SPL) of 122 dB (25 Pa) and above. Johannesen and Hodgson [10] examined the structure of weak shock waves in air from a gas-kinetics standpoint. Weak shock waves emanating from

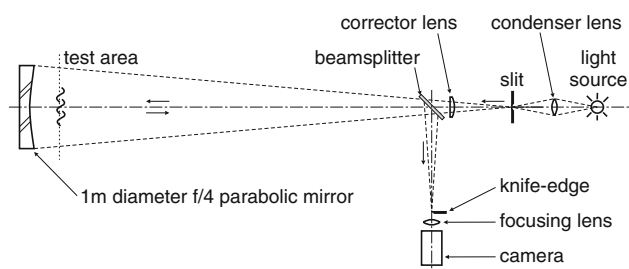


Fig. 1 Top-view layout diagram of Penn State's 1-m double-pass coincident schlieren system

brass musical instruments were observed by Hirschberg et al. [11] and Pandya et al. [12], while those produced by cracking a whip were most recently visualized by Krehl et al. [13], all using schlieren and shadowgraph techniques [14]. Finally, Mizukaki et al. [15] used digital phase-shift holographic interferometry to image weak shock waves in air at a SPL of 135 dB (112 Pa).

The goal of this paper is to further examine the visibility limits of loud sounds and weak shock waves in the atmosphere using a large, highly sensitive schlieren instrument and a high-speed digital camera. A second goal is to explore common phenomena that produce weak shock waves capable of being visualized in this manner.

2 Experimental methods and apparatus

Penn State's 1-m coincident double-pass schlieren system is fully described by Settles [14]. It features a 1-m diameter, $1/5$ -wave-accurate $f/4$ parabolic mirror as its single large optical component, diagrammed in Fig. 1. The sensitivity of this schlieren system is very good, better than $1/4$ arcsecond, owing to its effective optical lever-arm of 8 m and its double-pass arrangement.

For present purposes the schlieren illumination was provided by a 100 W ozone-free Newport-Oriel xenon arc lamp. A Photron APX-RS black-and-white digital camera recorded the schlieren image at frame rates from 10,000 to 30,000 frames/s with exposure times of 1 or 2 μ s. Since this camera has up to 6 s of real-time memory at high frame rates, most of the triggering and synchronization problems of the past are avoided. Instead, the camera's continuous recording process is simply stopped upon hearing the audible report of the phenomenon under study. A quick search of the last few seconds of recorded footage then provides the desired results.

In experiments to examine the visibility limits of loud sounds, a 4.8-cm diameter Insignia NS-S3000 4 Ω niobium microdome "tweeter" speaker with a frequency range of 3.5–20 kHz was positioned in the test area of the schlieren system. The speaker was driven by sinusoidal waveforms at 5, 10, and 15 kHz using a Simpson Model 422 function

generator and a consumer-grade stereo amplifier. SPL measurements were made with a CEL Instruments Ltd. Model 328 Sound Level Meter located opposite the speaker at a distance of 33 cm. This meter recorded peak C-weighted dB levels for each case tested. The field-of-view recorded at 30,000 frames/s and 2 μ s exposure by the APX-RS camera was rectangular and approximately 38 cm wide. A felt baffle was hung behind the sound level meter to reduce acoustic reflection. The Insignia NS-S3000 tweeter is rated to handle 100 W rms or 200 W peak power, but the only power-level data taken were the CEL-328 dB readings. However, some speakers were driven to destruction in order to achieve a SPL high enough for schlieren visibility.

3 Experiments on the schlieren visualization of loud sounds

The apparatus just described was used in an attempt to visualize loud sound waves in air. Eight tests were carried out at 5, 10, and 15 kHz with both SPL and schlieren results recorded. Success was achieved at the two higher frequencies, as shown by individual schlieren frames in Fig. 2. Note that the dB readings were taken at the left margin of each frame, so the actual SPL of the sound imaged between the speaker and the meter is higher than the recorded SPL. The CEL-328 meter itself was calibrated before the experiment, and is believed to be accurate to ± 2 dB.

While the raw schlieren results were unimpressive, at least something could be seen. The original images, recorded at 30,000 frames/s with 2 μ s exposure and 256×256 -pixel resolution, were thus image processed to enhance schlieren visibility. According to the philosophy espoused in [14], since contrast is central to schlieren sensitivity, digital post-processing should be applied as needed to bring out low-contrast features. In this case Adobe Photoshop CS2 software was used to first remove background gradients from the digital images by unsharp masking (amount 500%, radius 8.3 pixels, threshold 0 levels). Then a linear contrast stretch brightened the images, which typically used only the darker 180 of the 256 available gray levels in the raw state. Finally, a few distracting black-spot artifacts brought out by the unsharp masking were removed by hand to yield the images shown in Fig. 2.

At this schlieren sensitivity level, small thermal disturbances in the laboratory air compete with the sound field for visibility. Room ventilation was shut down and experimenter movement curtailed in order to limit this problem to the level shown in Fig. 2.

The quantitative results of these experiments are shown in Fig. 3 as a plot of SPL versus sound frequency. Clearly, based on both Figs. 2 and 3, sound becomes easier to see by schlieren imaging as the frequency increases. This is

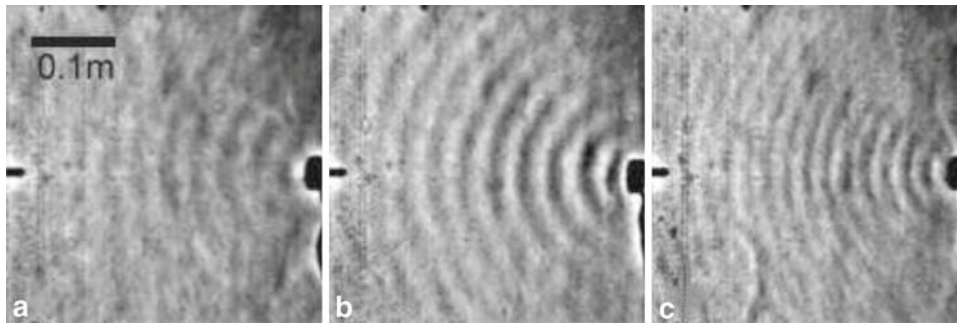


Fig. 2 Schlieren images of sound waves from a speaker in air at frequencies (f) and peak SPL of **a** $f = 10$ kHz, SPL = 109.2 dB, **b** $f = 10$ kHz, SPL = 119.8 dB, **c** $f = 15$ kHz, SPL = 102.5 dB. In each frame the speaker is at the *right* and the sensor of the SPL meter is at

the *left*, separated by a distance of 33 cm. In frame **c** there is thermal interference in the *lower left* quadrant and a thermal plume rising from the speaker itself

understandable in that the refractive-index gradient, thus schlieren visibility, produced by the sound wave must grow stronger in higher-frequency (shorter-wavelength) sound if the acoustic power level is held constant. In other words, the product of the sound frequency f and amplitude ΔP must remain constant in order to maintain constant schlieren visibility. This can be expressed as a visibility criterion, first recalling the standard definition of the SPL:

$$\text{SPL} = 20 \log \frac{\Delta P}{P_{\text{ref}}} \quad (1)$$

where P_{ref} has the standard value of 0.00002 Pa, and then writing:

$$f \cdot P_{\text{ref}} \cdot 10^{\frac{\text{SPL}}{20}} = \text{constant} \quad (2)$$

where the value of the constant corresponding to the presently observed limit of sound visibility from Fig. 3 is 35,000 Pa/s. The value of this constant is dependent on the schlieren optics used and should be experimentally determined for a given schlieren system. For a further discussion of schlieren sensitivity the reader is referred to [14].

Equation (2) is shown as a straight line in Fig. 3, dashed above SPL ≈ 105 dB. The reason for this, as described in Hamilton and Blackstock [16], is that a sinusoidal linear sound wave becomes distorted as its amplitude is increased into the nonlinear regime, where the wavefronts steepen to eventually form distinct shock waves. Equation (2) is no longer correct in this case, and a proper extension of the dashed line shown in Fig. 3 to lower frequencies should become concave downward in order to indicate the increased visibility of weak shock waves over linear sound at higher SPL.

Such a schlieren visibility curve was also proposed by Bucaro and Dardy [8], and is also given in Fig. 3. It shows the concave-downward behavior just described, but asymptotes to a slope similar to that of (2) at high sound frequencies. Unfortunately Bucaro and Dardy did not publish the derivation of their visibility curve. Nevertheless it is clear

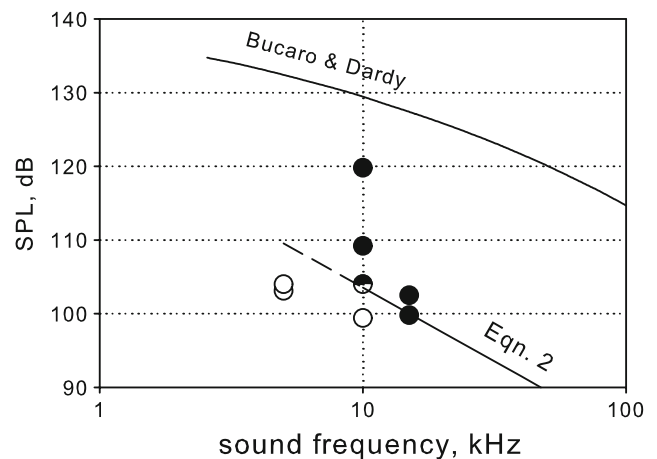


Fig. 3 Semilogarithmic plot of SPL versus sound frequency. *Filled symbols* represent current experiments wherein schlieren visualization of the sound field succeeded, while *open symbols* show where it failed

that their threshold of sound visibility to schlieren optics lies at a much-higher SPL, some 30 dB higher, than in the present case. They describe their optics as a “diffraction-limited schlieren system with a 15 cm aperture”. Assuming that they used $f/10$ mirrors or lenses, their system would have had less than 1/10th the sensitivity of the present schlieren optics based solely on size and single- versus double-pass design. This is believed to account for some, if not all of the discrepancy in sound visibility limits shown in Fig. 3.

The upshot of Fig. 3 is that we can show how sound visibility to schlieren optics varies with frequency, but the threshold SPL at which sound becomes visible is highly dependent upon the sensitivity of the optical system that one employs.

4 On the schlieren visualization of very weak shock waves

The classical Rankine–Hugoniot (R–H) theory [17] provides an exact solution for shock waves of any strength in a perfect gas (taken here to have the ratio of specific heats $\gamma = 1.4$ for

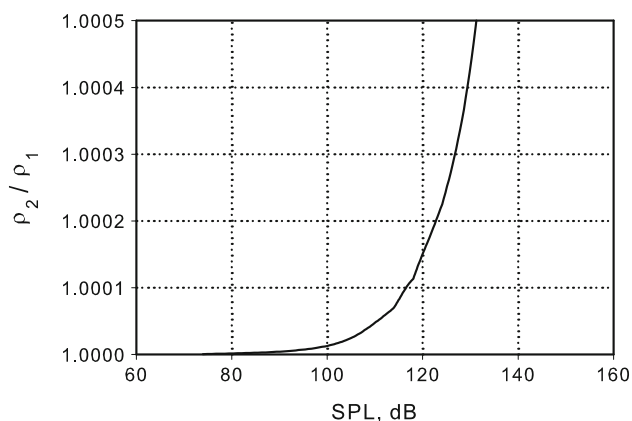


Fig. 4 Density ratio versus sound pressure level of a weak normal shock per Rankine–Hugoniot theory with $\gamma = 1.4$

atmospheric air). Thus the expression for the static density ratio across a normal shock:

$$\frac{\rho_2}{\rho_1} = \frac{(\gamma + 1)M_1^2}{(\gamma - 1)M_1^2 + 2} \quad (3)$$

can be examined in order to explore the density-gradient behavior as the shock-wave Mach number, M_1 , tends toward unity and the shock wave tends toward a sound wave. M_1 , though, lies so close to unity ($1.0000 < M_1 < 1.0005$) in the region of present interest that a more meaningful index of shock strength is needed. That is provided by the SPL already defined in (1), where ΔP now represents the static pressure jump across the shock:

$$\frac{P_2}{P_1} = \frac{P_{\text{atm}} + \Delta P}{P_{\text{atm}}} = \frac{2\gamma M_1^2 - (\gamma - 1)}{\gamma + 1} \quad (4)$$

where the atmospheric pressure, P_{atm} is taken to be 101.325 kPa.

Based on (1)–(4) the shock wave density ratio is plotted versus the corresponding SPL in Fig. 4 over the specified weak Mach number range in air. From this point-of-view, below a SPL of about 100 dB phenomena are essentially incompressible and thus no optical visualization can be expected. But the curve has a pronounced “knee” in the range of $100 < \text{SPL} < 120$ dB ($2 < \text{Pa} < 20$), and thereafter the density ratio rises quickly with further shock strength. Based solely on this result, and assuming unlimited optical sensitivity, we might expect to begin to see shock waves in air in the $100 < \text{SPL} < 120$ dB range, as was already demonstrated in Figs. 2 and 3. Whether one uses the term “shock wave” or “sound wave” in this range is more a matter of semantics than substance.

The $100 < \text{SPL} < 120$ dB range is often typified by loud concert music, jet aircraft noise at a distance, and gasoline-powered equipment nearby. The US Occupational Safety and Health Administration (OSHA) permits such sound exposure in the workplace for only a few minutes per day.

Next consider the weak-shock-wave structure in this range, since schlieren optics reveals the density gradient $\partial\rho/\partial x$, which is approximately the density jump $\Delta\rho = \rho_1(\rho_2/\rho_1 - 1)$ divided by the shock thickness Δx . Here we cannot assume, as is usual for strong shock waves at one atmosphere, that Δx is less than the wavelength of visible light. In fact, it turns out that a strong-shock-wave-like density gradient is not to be expected in the $100 < \text{SPL} < 120$ dB range.

This matter was taken up in 1979 by Johannesen and Hodgson [10], who wrote a thorough review of weak-shock-wave structure in the atmosphere. Briefly, they showed that this structure is determined by molecular vibration, which can lead to overall weak shock-wave thicknesses ranging from less than a centimeter to over a meter for the weakest waves. A shock wave with a thickness of one meter would be well below the detection limit and larger than the aperture of essentially all practical schlieren optics [14]. The matter is complicated by differences in O_2 and N_2 behavior and a substantial dependence upon the initial air temperature and humidity. Their worked examples include a very weak shock wave with $\Delta P = 10$ Pa (SPL = 114 dB) in 295 K air with 50% relative humidity. According to Lighthill’s [18] terminology this wave is “fully dispersed”, i.e., it has a smooth transition between end states over a finite thickness with no discrete jump in properties. Its detection by schlieren optics is thus expected to require exceptional sensitivity. A stronger shock-wave example with $\Delta P = 30$ Pa (SPL = 123.5 dB) and the same initial conditions develops a cusp-like profile, though still no discrete jump. This should nonetheless be detectable as an incipient shock wave, given reasonable schlieren sensitivity. Johannesen and Hodgson’s [10] strongest example has $\Delta P = 110$ Pa (SPL = 134.8 dB), where a small discrete property jump is followed by a long vibrational relaxation zone: a “partly dispersed” wave [18]. This case is strong enough for the density jump to be visible to schlieren optics as a familiar, discrete shock wave.

5 Experiments on the schlieren visualization of shock waves from common phenomena

Given the ability, described above, to image loud sounds and weak shock waves, we have explored a range of common phenomena thought to produce SPLs sufficiently high to be visible to our schlieren apparatus. These can be broadly categorized as: (1) brass musical instruments, (2) impact phenomena which compress a bubble of air that, upon subsequent expansion, drives a shock wave, (3) other pressure-release phenomena, and (4) phenomena that involve local supersonic motion of an object with its attendant shock wave. Note that explosions, gunshots, etc. are covered elsewhere, e.g.

[19–21], and are not considered to be within the scope of the weak everyday phenomena visualized here.

5.1 Shock waves from a trumpet

Pandya et al. [12] earlier used the present schlieren apparatus to examine shock waves produced by loud, high-pitched trumpet notes. Under such circumstances there is a shock-tube-like effect of the performer's intermittent breath pressure driving the cylindrical duct of the instrument, and visible weak shocks are seen emanating from the trumpet flare as shown in Fig. 5. SPL measurements revealed 118–124 peak dB(A) levels associated with these shock waves.

5.2 Shock waves due to impact compression

5.2.1 Snapping a leather belt

Before the era of computers and video games, children amused themselves with whatever materials they had at hand. A very old form of such amusement involves folding a leather belt at mid-length to form a loop. The ends of this loop are grasped in both hands, and are pulled outward sharply in order to snap the leather together. With a little practice this can produce a loud “crack” with which to startle others. Any such sharp, startling “crack-like” sound is a possible shock wave, since that is how our ears and brains interpret a step-wise overpressure in the air. (A supersonic bullet produces the same sensation [22].) Using the equipment described earlier we have imaged a dozen belt snaps, as exemplified in Fig. 6.

During the snap, as the leather begins to make contact (Fig. 6a), air is trapped and compressed first near one hand or near the other at random. The ejected compressed air drives a shock wave that propagates along the belt from one hand to the other (e.g. from left to right in Fig. 6a–c) and then reflects. This shock appears to be circularly symmetric in the side view shown in Fig. 6d. In some cases a second, later shock appears, and in some of the image sequences the turbulent air that drove the shock wave is seen still escaping from the belt-snap well after the shock has dissipated.

5.2.2 Snapping a ruler on a table

A table, desk, or other flat surface is sharply struck broadside by a common 12-in. (30.5 cm) ruler or a wooden meter-stick, creating once again a loud snap or crack. In much the same way as in the belt-snap, air is trapped between the impacting surfaces and is momentarily compressed, possibly to several atmospheres. This compression typically begins opposite the end of the ruler that is held, and in our experiments runs along the length of the ruler fast enough to produce one or a series of oblique shock waves, as shown in Fig. 7. It is quite easy to produce relatively strong home-made shock waves this

way: in our high-speed videos the resulting shocks reflected from the laboratory wall outside the field-of-view and were still strong enough to be seen crossing in front of the schlieren mirror a second time. Also, as in the belt-snap, turbulent ejected compressed air can be seen in the impact region after shock-wave formation.

5.2.3 Dropping a book on a table

A heavy book is held horizontally about 1 m above a table and dropped so that it makes approximately a flat impact (i.e., not edge-on). As shown in Fig. 8, the attitude of the book prior to impact need not be perfectly parallel to the table, and that is in any case difficult to achieve. A sharp audible report is heard upon impact. With present equipment, the ejected compressed air between the book and the table is clearly visible in the form of a vortex, along with the driven shock. A similar vortex is produced in the belt-snap experiment, but it is less coherent and not as easily observed due to the hands in the images.

5.2.4 Clapping the hands

The sound of applause is generated by compressing air between the cupped palms of the hands upon their impact with one another. Occasionally, in the theater or concert hall, an enthusiastic hand-clapper can inflict auditory pain on those around him. This pain, and the temporary hearing desensitization that can accompany it, is a suspected result of shock waves in the air caused by the clapping hands. To explore this, we have observed several hand-claps with the current schlieren apparatus. The most successful visualization is shown in Fig. 9. Shock waves are indeed generated but they are very weak. As in Fig. 2, a severe unsharp mask has been applied to these images in order to bring out the shocks for publication. Even so, they are almost buried in the turbulent convection from the hands. We did not pursue this issue further, but we speculate that, if a hand-clapper of sufficient annoyance could be recruited, the resulting shock waves would be notably stronger than those shown in Fig. 9.

5.3 Other pressure-release phenomena

Shock waves driven by gas expansion can also occur without requiring physical impact if the gas is released from a storage reservoir. Two common examples are bursting a toy balloon and popping the cork of a champagne bottle.

The former has been photographed before on various occasions (e.g. [23]), but a new example is shown here as well, for completeness, in Fig. 10. In this example we used argon gas rather than air to fill the ordinary toy balloon, purely to improve the schlieren visualization of the gas. The balloon self-burst well before it was fully distended, driving a

Fig. 5 Schlieren images of shock waves observed while playing trumpet notes. **a** Mezzo-forte high G, **b** fortissimo middle C, **c** fortissimo high G. The outer diameter of the trumpet flare is 12.2 cm. The performer's turbulent breath is also seen emerging from the instrument [12]

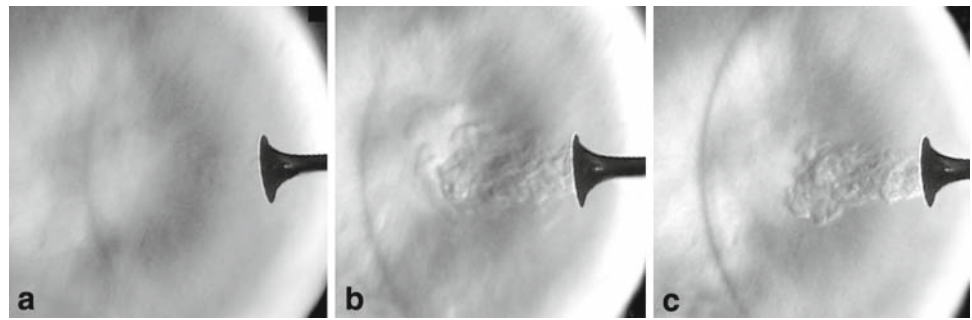


Fig. 6 Schlieren frames of belt-snap shock waves. **a–c** Front view and **d** side view. The SPL meter shown to the *left* in **d** recorded peak SPLs of 103–120 dB in repeated trials. Frames **a–c** are separated by 0.2 ms and frame **d** is from a different trial

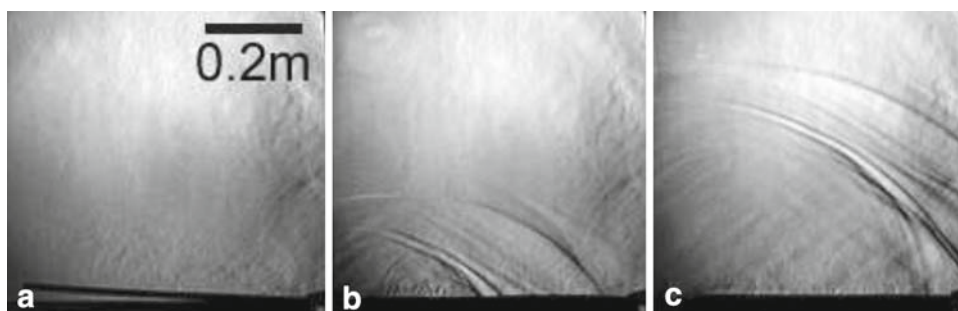
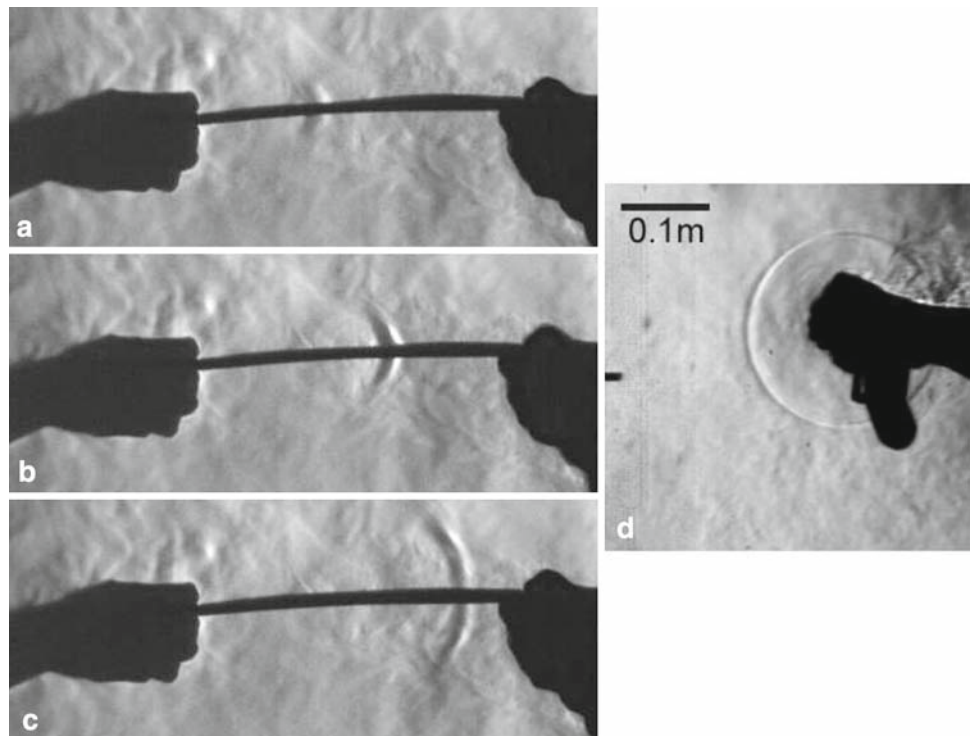


Fig. 7 Schlieren frames of ruler-snap shock waves. **a** The ruler has impacted the table at the *bottom right* and its *left* end is about to impact. **b** 2.7 ms later a system of shock waves is observed running *left-to-right*.

c 0.7 ms later the shock system moves out of the field-of-view to the *right*. Turbulence near the impact at the *bottom* of frames **b** and **c** denotes ejected compressed air between the ruler and the table

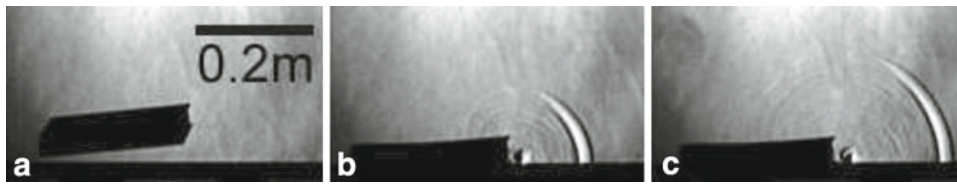


Fig. 8 Schlieren frames of the impact of a book on a table. **a** The book appears prior to impact, its *left front corner* nearest the table. **b** 127 ms later, compressed air beneath the *right edge* of the book is ejected,

driving a double-shock front that diffracts around the *top* of the book. **c** 0.2 ms later the shock system moves out of the frame to the *right*. Note some flexure of the book upon impact

Fig. 9 Schlieren frames of clapping the hands. **a** An early frame showing the hands coming together before the clap. **b** Very weak shock wave motion to the right of the hands and **c** 0.5 ms later the generated sound/shock waves move away from their source. The turbulence visible in these frames is thermal convection from the hands

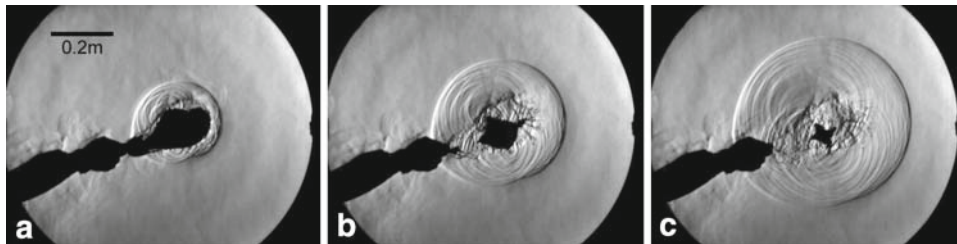
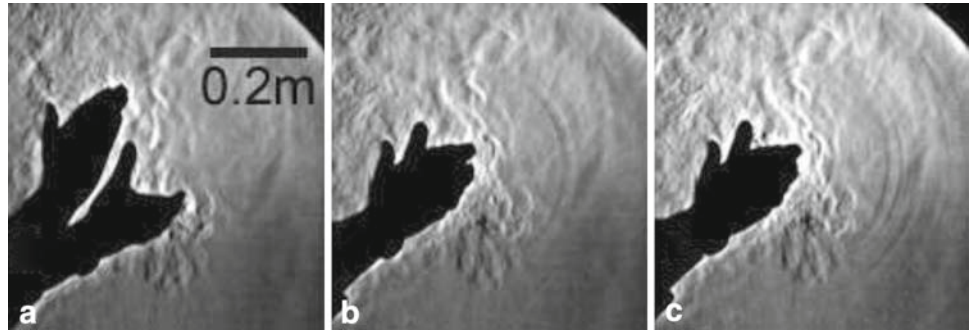


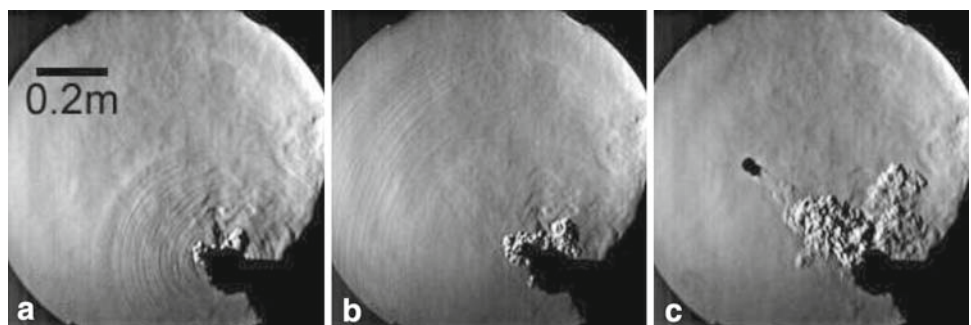
Fig. 10 The burst of an argon-filled toy balloon, recorded at 12,000 frames/s. **a** The bowling-pin-shaped balloon skin has begun to unwrap about 0.25 ms after the start of the burst, driving a shock wave

into the surrounding air. **b** 0.17 ms later, the contact surface between argon and air is revealed. **c** 0.17 ms later the primary shock front, reinforced by many secondary compressions, becomes almost spherical

relatively strong primary shock wave followed by numerous secondary waves, all clearly visible at the current schlieren sensitivity level.

Popping the cork of a bottle of champagne does not produce the same sharp “crack” sensation described earlier, so a single explicit shock wave is not expected. Indeed, the gas-venting process (Fig. 11) is seen to proceed slowly enough to produce only a dispersed wave train. No SPL or other quantitative data were collected during this experiment, but by comparison with Fig. 2 the dominant frequency of this wave train appears to be higher than 20 kHz.

Fig. 11 Popping the cork of a champagne bottle, recorded at 10,000 frames/s. **a** 0.8 ms after the beginning of the pop, a train of high-frequency waves propagates into the air. The gas exiting the bottle around the base of the cork is also visible. **b** 1.0 ms later, the sound of the pop moves away. **c** 16 ms later the acoustic event is long past but the flight of the cork continues



5.4 Phenomena involving local supersonic motion of an object

The auditory sensation of breaking a wooden stick is shock-wave-like, but Fig. 12 reveals only a wave train similar to that just seen from popping the cork of the bottle of champagne. For this purpose dead dry tree branches of 2–3 cm diameter were used in several trials. The entire process of acoustic emission lasts about 5 ms, so it appears that the wooden fibers are failing sequentially over this interval rather than all at once.

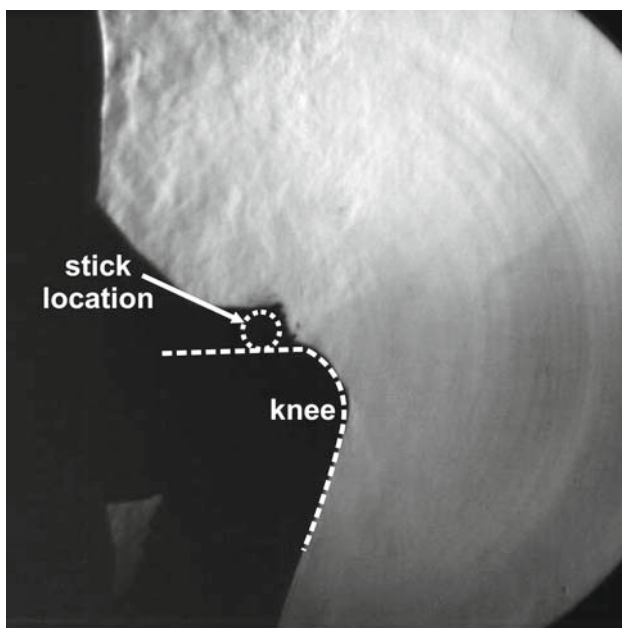


Fig. 12 Snapping a wooden stick across the knee, centered about mid-frame and recorded at 10,000 frames/s. This frame is from an early stage of the snap, where the initial acoustic emission has yet to leave the field of view. The turbulence within the image is due to the human thermal plume

Krehl et al. [13] have given a thorough description and historical perspective of whip cracking, along with images of the shock wave generated by the local supersonic motion of the whip-tip (see also McMillen and Goriely [24]). Locker-room lore has it that something similar occurs when a wet towel is snapped, with painful results for anyone who gets in the way. We were able to confirm this by snapping an old, wet, frayed towel in the test area of the present schlieren equipment (Fig. 13). This is not easy to do even with a whip [24], let alone a towel. Nonetheless the shock-wave at the tip of a well-snapped towel is more than strong enough to visualize with the current apparatus. As shown here, multiple shocks can be produced as individual parts of the frayed tip are accelerated during the snap.

6 Conclusions

From this exercise in weak-shock-wave visualization in the air we have observed that there are many common phenomena producing density gradients sufficiently strong to be rendered visible to a sensitive schlieren system. Several others have been suggested but not yet tried. There is the potential here to reveal interesting and useful new physical phenomena, and to investigate the sound fields produced by all sorts of commercial equipment. For future work, additional quantitative measurements including acoustic spectra are needed.

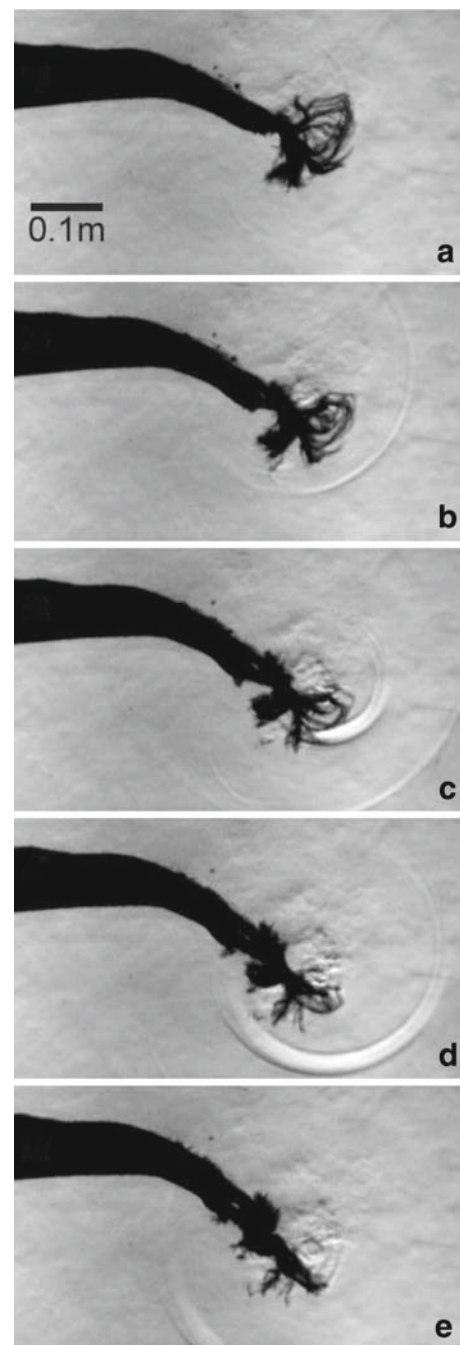


Fig. 13 Shock wave generation from the rotation of the frayed end of a snapped wet towel. Multiple shock waves are produced as the frayed tip rotates. The images are separated by 0.2 ms

Due to the vanishing strength of many of these phenomena, image processing of the schlieren results was critical. While we show that loud-sound visibility improves with frequency as expected, the threshold SPL for visibility is highly dependent upon the sensitivity of the optical system and image post-processing.

The phenomena visualized here include: (1) brass musical instruments, (2) impact phenomena which compress a bubble of air that, upon subsequent expansion, drives a shock wave, (3) other pressure-release phenomena, and (4) phenomena that involve local supersonic motion of an object with its attendant shock wave. Several of these were observed to produce a train of high-frequency sound waves rather than discrete shock waves. It could be that lower frequencies were also present but not visible for the reason mentioned above, but the physics of these examples nevertheless deserves further scrutiny.

Acknowledgments We thank our colleagues R. P. Bigger, M. M. Biss, L. J. Dodson, M. J. Lawson, T. J. Liebner, J. D. Miller, and J. A. Volpe for their assistance.

References

- Krehl, P., Engemann, S.: August Toepler—the first who visualized shock waves. *Shock Waves* **5**, 1–18 (1995)
- Foley, A.L., Souder, W.H.: A new method of photographing sound waves. *Phys. Rev.* **35**, 373–386 (1912)
- Miller, D.C.: *Sound Waves: Their Shape and Speed*. Macmillan, New York (1937)
- Wood, R.W.: Photography of sound waves by the schlieren methode. *Philos. Mag.* **48**, 218–227 (1899)
- Sabine, W.C.: Theatre acoustics. *Am. Archit.* **104**, 257 (1913)
- Kock, W.E.: *Seeing Sound*. Wiley-Interscience, New York (1971)
- Darius, J.: Visions of sound: acoustic field visualization by schlieren color photography. *New Sci.* **62**, 408–414 (1974)
- Bucaro, J.A., Dardy, H.D.: Visualization of ultrasonic waves in air. *J. Acoust. Soc. Am.* **62**, 1506–1507 (1977)
- Bershader, D., Prakash, S.G.: Improved flow visualization by use of resonant refractivity. In: *Proceedings of the 14th AIAA Aerospace Sciences Meeting*, Washington DC, Paper 76–71 (1976)
- Johannesen, N.H., Hodgson, J.P.: Physics of weak waves in gases. *Rep. Prog. Phys.* **42**, 629–676 (1979)
- Hirschberg, A., Gilbert, J., Msallam, R., Wijnands, A.P.L.: Shock waves in trombones. *J. Acoust. Soc. Am.* **99**, 1754–1758 (1996)
- Pandya, B.H., Settles, G.S., Miller, J.D.: Schlieren imaging of shock waves from a trumpet. *J. Acoust. Soc. Am.* **114**, 3363–3367 (2003)
- Krehl, P., Engemann, S., Schwenkel, D.: The puzzle of whip cracking—uncovered by a correlation of whip-tip kinematics with shock wave emission. *Shock Waves* **8**, 1–9 (1998)
- Settles, G.S.: *Schlieren and Shadowgraph Techniques: Visualizing Phenomena in Transparent Media*. Springer, Berlin (2001)
- Mizukaki, T., Kleine, H., Takayama, K.: Quantitative visualization of weak shock waves by phase-shift holographic interferometry. In: *Proceedings of the 23th International Symposium on Shock Waves*, Arlington, Texas, Paper 1904, pp. 410–417 (2001)
- Hamilton, M.F., Blackstock, D.T. (eds.): *Nonlinear Acoustics*. Academic Press, New York (1998)
- Shapiro, A.H.: *The Dynamics and Thermodynamics of Compressible Fluid Flow*. Ronald Press, New York (1953)
- Lighthill, M.J.: Viscosity effects in sound waves of finite amplitude. In: Batchelor, G.K., Davies, R.M. (eds.) *Surveys in Mechanics*, pp. 250–351. Cambridge University Press, London (1956)
- Hargather, M.J., Settles, G.S.: Retroreflective shadowgraph technique for large-scale flow visualization. *Appl. Opt.* **48**, 4449–4457 (2009)
- Settles, G.S.: High-speed imaging of shock waves, explosions and gunshots. *Am. Sci.* **94**, 22–31 (2006)
- Hargather, M.J., Settles, G.S.: Optical measurement and scaling of blasts from gram-range explosive charges. *Shock Waves* **17**, 215–223 (2007)
- Haag, L.C.: The sound of bullets. *Assoc. Firearm Toolmark Exam. J.* **34**, 255 (2002)
- Kleine, H., Settles, G.S.: The art of shock waves and their flow-fields. *Shock Waves* **17**, 291–307 (2008)
- McMillen, T., Goriely, A.: Whip waves. *Phys. D* **184**, 192–225 (2003)